Journal of Hazardous Materials 196 (2011) 360–369

Contents lists available at SciVerse ScienceDirect

Journal of Hazardous Materials

journal homepage: www.elsevier.com/locate/jhazmat

Synthesis and characterization of activated carbon from sawdust of Algarroba wood. 1. Physical activation and pyrolysis

Juan Matos*, Carol Nahas, Laura Rojas, Maibelín Rosales

Engineering of Materials and Nanotechnology Centre, Venezuelan Institute for Scientific Research (IVIC) 20632, Caracas 1020-A, Venezuela

ARTICLE INFO

Article history:
Received 7 April 2011
Received in revised form 2 September 2011
Accepted 10 September 2011
Available online 16 September 2011

Keywords:
Activated carbon
Physical activation
Pyrolysis
Algarroba wood

ABSTRACT

Synthesis of activated carbon (AC) from sawdust of Algarroba wood was performed as a function of the temperature under CO_2 and N_2 flow. Characterization was performed by adsorption–desorption N_2 isotherms, FTIR, XPS and SEM. Functional acid or basic groups were detected on the surface of AC. For both studied atmospheres, the maximum value of surface area was obtained at 800 °C. A monotonic correlation between temperature and mean pore diameter was detected being the higher the activation temperature the lower the mean pore width of AC. Ultramicroporous AC with pore diameters of 6.7 Å and 5.3 Å were obtained at 900 °C under CO_2 and N_2 flow, respectively. It can be concluded that pore diameter and the functionalization of the AC surface can be controlled easily controlling the temperature of activation, independently of the gas atmosphere. The present results suggest that waste biomass is a potential source for the synthesis of carbon materials with potential novel applications.

1. Introduction

The lignocelluloses are the most common precursor materials to obtain activated carbon (AC) of low cost [1–8]. AC has been used extensively as adsorbent and catalytic support mainly due to the high surface area up to 3000 m^2/g and a wide range of pore sizes [1]. AC has been studied in catalytic heterogeneous reactions such as hydrogasification [9,10], hydrodesulphurization [11,12] and photocatalytic detoxification of waste waters [13–15]. The efficiency of AC is associated directly with texture and surface properties [16,17]. An increasing interest of wood-derived carbon-supported catalysts has been performed, mainly upon the kinetics of methane conversion reactions [18–22] to obtain syngas, bio-oil and as feedstock for chemical production. These works showed that physical and chemical characteristics of carbon supports influence the catalytic activity. Therefore, the kinetics parameters related with the synthesis of AC from biomass such as sawdust from wood [8,23–26] has received much attention. As part of a project aimed to obtain up-grading materials from biomass, the principal aim of this work treats with the synthesis of carbon materials from the sawdust of Algarroba wood. Discussion about the influence of the gaseous atmosphere and of the temperature of reaction on the texture and the chemical surface properties of the carbon are also presented.

2. Experimental

2.1. Raw material and activated carbon characterization

Sawdust from Algarroba (Hymenaea Courbaril) wood was employed. It was firstly crashed and sieved before characterization. The mean size of particles was 350 μm. Tests of moisture at 120 °C by 2 h, ash at 550 °C by 14 h, and volatiles at 850 °C by 7 min were also performed. Bulk density was estimated by geometrical filled method with sieved microparticles of 350 μm. Atomic absorption (AA) was performed to analyze the chemical composition of ashes. Textural characterization was performed by adsorption–desorption N_2 isotherms at 77 K. The full isotherms in the range of 4×10^{-3} to 84 kPa were measured in a ASAP-2020 equipment (Micromeritics). Equivalent surface area, micropore area and volume, total pore volume and pore diameters were obtained by Brunauer–Emmet–Teller (BET), Harkins–Jura (HJ) and Horvath–Kawazoe (HK) methods, respectively. These methods were employed because carbon materials can contain slits and spherical pores [26]. Fourier-transform infrared spectroscopy (FTIR), X-ray photoelectronic spectroscopy (XPS), and scanning electron microscopy (SEM) were also performed to characterize the samples. FTIR spectrums were obtained on a spectrophotometer Magna-IR 560 from Nicolet. The powders were mixed with KBr in a 5% (w/w) mixture and pressed to tablets of 1 cm diameter at 10 t for 1 min. Spectra were recorded from 4000 to 400 cm^{-1} with a resolution on 5 cm^{-1}. XPS was carried out in an ESCALAB 220i-XL spectrometer (VG scientific) equipped with a hemispherical electron analyzer and a double anode Mg–Al

* Corresponding author. Tel.: +58 212 5041166; fax: +58 212 5041166.
E-mail addresses: jmatos@ivic.gob.ve, jmatoslale@gmail.com (J. Matos).

0304-3894/$ – see front matter © 2011 Elsevier B.V. All rights reserved.
doi:10.1016/j.jhazmat.2011.09.046

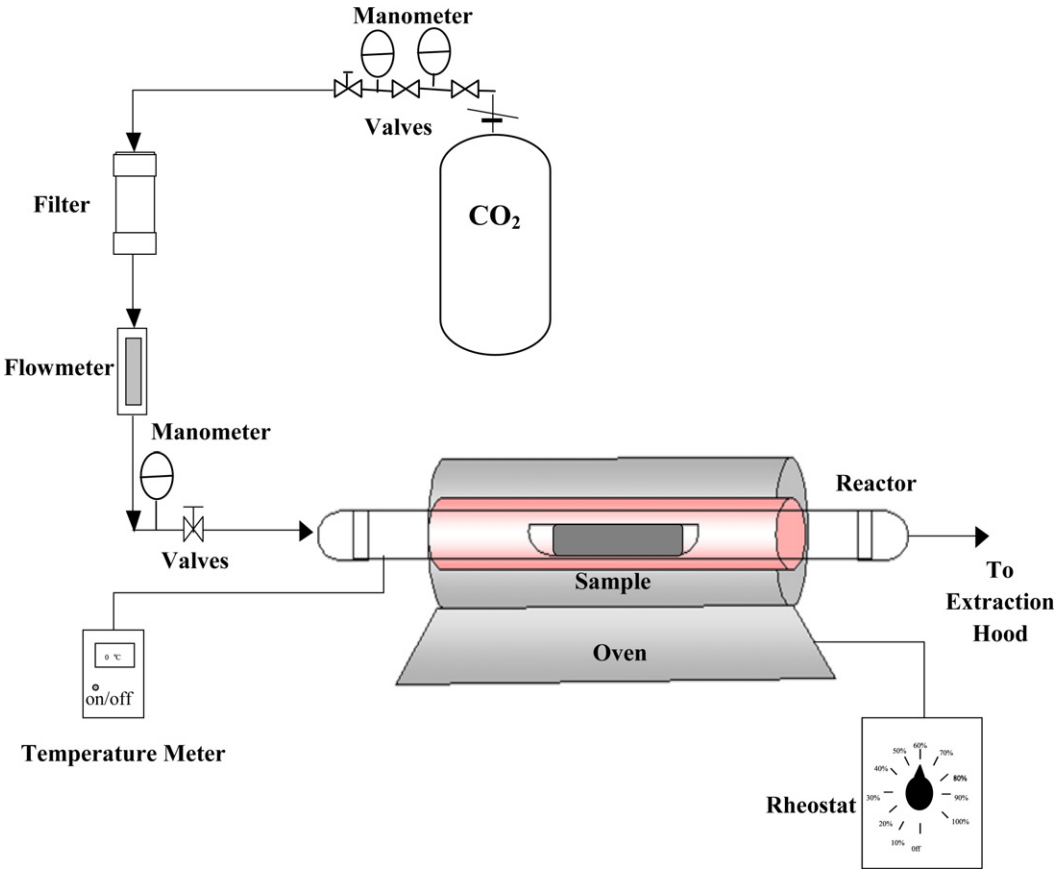

Fig. 1. Scheme of activation set-up.

non-monochromatic X-ray source. The pressure in the analysis chamber was kept below 10^{-9} Torr. The data were corrected to the C1s level at 285.0 eV. Scanning electron microscopy (SEM) images were obtained from palladium–gold-coated samples in a XL-30 microscopy from Phillips.

2.2. Physical activation and pyrolysis of sawdust

Carbon samples were prepared in one-step procedure by two different ways, physical activation under CO_2 flow and by pyrolysis under inert N_2 flow. All samples were thermally treated by 0, 1 or 2 h at the final temperature (200 °C up to 900 °C) and denoted AC_{CO_2-T} and AC_{N_2-T}, with T the final temperature. In a typical synthesis [16], 3 g of sieved wood was treated thermally under CO_2 or N_2 flows (100 mL min^{-1}) at constant heating rate (10 °C/min) from ambient to final temperature. Activation was carried out at nearly constant atmospheric pressure (100 kPa) inside a tubular kiln (Heraeus). Fig. 1 shows a schematic representation of the equipment used in this work. Tubular reactor was made of stainless steel or Pyrex glass depending of final temperature. Different reaction time (0, 1 and 2 h) was followed and then the oven was left cooled to temperature environment under flow of inert gas. The yield (%) of carbon was verified after each experiment.

2.3. Phenol photodetoxification

Phenol was purchased from Aldrich. The photocatalyst was TiO_2 Degussa P25, mainly anatase (ca. 70%) under the shape of non-porous polyhedral particles of ca. 30 nm mean size with a surface area of 50 m^2/g. Activated carbons prepared under CO_2 and N_2 flow at 800 °C and 1 h were selected for the study because they showed the highest surface areas (discussed below). These samples were denoted: TiO_2–AC_{CO_2} and TiO_2–AC_{N_2}. The experimental set-up has been described before [13,14] but it can be summarized as follows. The batch photoreactor was a cylindrical flask made of Pyrex of ca. 100 mL with a bottom optical window of ca. 4 cm diameter and was open to air. Irradiation was provided by a high pressure mercury lamp (Phillips HPK 125 W) and was filtered by a circulating-water cell (thickness 2.2 cm) equipped with a 340 nm cut-off filter (Corning 0.52). The water cell was used to remove all the IR beams, thus preventing any heating of the suspension, especially in the presence of black activated carbon. The cut-off filter, although decreasing the overall UV-light power available, enables one to eliminate any photochemical side reaction. Millipore disks (0.45 μm) were used to remove particulate matter before HPLC analysis. The HPLC system comprised a LDC/Milton Roy Constametric 3200 isocratic pump and a Waters 486 tunable absorbance detector (Millipore) adjusted at 270 nm for the detection of phenol. The quantity of 50 mg of Titania was chosen since in our conditions there is a full absorption of the UV light entering the photoreactor and because it has shown a optimum of composition in the photodegradation of phenol [13]. The quantity of 10 mg AC was chosen to ensure a good adsorption of phenol related to the high surface area of AC without disturbing the UV absorption by titania nor phenol adsorption on it [13]. Samples of the suspension were removed at regular intervals for analysis and from the linear regression of the kinetic data of phenol disappearance as a function of reaction time $Ln(C_o/C_t) = f(t)$, the first-order apparent rate-constants ($k_{app\text{-}phenol}$) were obtained to compare the photoefficiency of the TiO_2–AC against TiO_2 alone. Further details can be verified elsewhere [13].

Table 1
Characterization of Algarroba (*Hymenaea Courbaril)* wood.

Moisture (wt%)	9.8 ± 0.4
Ash (wt%)	1.30 ± 0.04
Volatiles (wt%)	72.1 ± 0.7
Fixed carbon (wt%)	16.8 ± 1,3
Bulk density (g/cm^3)	0.89 ± 0.03

3. Results and discussion

3.1. Raw material characterization

Results of wood characterization are shown in Table 1. It is well-reported [1,2] that carbon yield is affected by many factors such as the precursor material, the activation method, the activation agent, and other activation parameters such as pressure and heating rate. In addition, the high volatile content (about 72%) would suggest low yields during the synthesis in agreement with the low fixed coal of about 17% (Table 1). A low content of ash of about 1.3% was detected in the composition of the wood, suggesting that the carbon materials will have a high purity. Table 2 shows a summary of the results of atomic absorption (AA) obtained from ashes of Algarroba. Alkaline and alkaline-earth metals were detected being Ca the most important (ca. 0.4%). Also, low content of amphoteric elements (Al and Si) and first row transition metals (Cr, Cu, Fe, Ni, Zn and Mn) were detected. However, this composition is low enough (less than 0.1%) that any catalytic influence of transition metals on the thermal degradation of the wood can be rejected.

It should be pointed out an important quantity of phosphor (ca. 0.7%) in the composition of wood. Laine et al. [27] have reported that P found in AC obtained from coconut shell is structured commonly in the shape of cyclic or linear polyphosphates $[(P_nO_{3n})]_n$- and $[(P_nO_{3n+1})]_{(n+2)}$-, respectively. These phosphates can be intercalated in the borders of the carbon sheets with a strong interaction between the anions phosphates and the carbon atoms.

3.2. Thermal degradation of wood

The yield (%) after thermal degradation (followed gravimetrically) under CO_2 or N_2 flow is show in Fig. 2A and B, respectively. The moisture corresponding to the heating up to 120 °C is also observed in Fig. 2. It can be noticed that the thermal decomposition begins on 200 °C in both gaseous atmospheres with burn-off of about 12% and 10% under CO_2 and N_2 flow, respectively. This is in agreement with previous works of thermal decomposition of lignocelluloses materials [23,24,28]. Fig. 2 shows three thermal different degradation zones as a function of temperature. These zones can be identified at low, moderate and high temperatures as follows. The low temperature zone between 200 and 300 °C, the moderate one between 350 and 600 °C, and the high temperature zone between 600 and 900 °C. For the case of the thermal degradation under CO_2 atmosphere, Fig. 2A shows that the higher the activation temperature and reaction time the lower the yield and concomitantly the highest burn-off of about 94% and 70% under CO_2 and N_2, respectively. In short, up to 600 °C, the burn-off follows a very similar trend under both atmosphere, but at temperature higher than 600 °C, the burn-off is clearly larger under CO_2 because the carbonized wood reacts in an efficient way with CO_2 to major temperatures that 690 °C according to Boudouard's reaction [29]: $C + CO_2 \rightarrow 2CO$, which is a bimolecular process. In addition, the pyrolysis under N_2 flow (Fig. 2B) shows a similar behavior up to 700 °C but then being a constant to temperatures higher than 700 °C. By contrast, under the atmosphere of N_2 the unimolecular thermal decomposition of the wood happens from temperatures of 200 °C up to 700 °C. At higher temperatures than 700 °C and under inert atmospheres, the yields remain practically constant because of the aromatization of carbon atoms into graphite sheets [30–33].

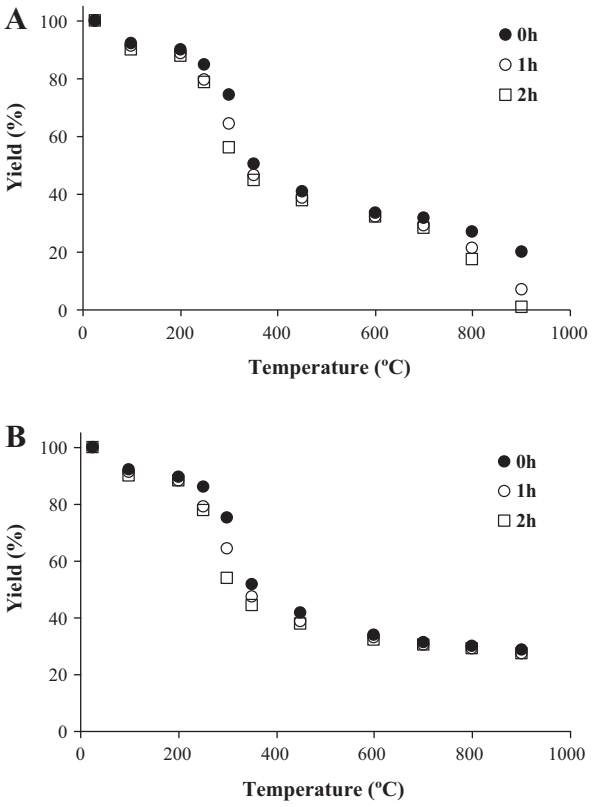

Fig. 2. Yields of Algarroba wood as function of temperature and reaction time. (A) Activation under CO_2 flow and (B) activation under N_2 flow.

Table 2
Atomic absorption analysis of ashes from Algarroba wood.

Element	Concentration in ashes (mg/L)	Proportion (%)	Wood composition (wt%)
Al	18.31	1.05	0.0136
Ba	0.51	0.03	0.0004
B	1.83	0.10	0.0014
Ca	538.46	30.80	0.4066
Cr	0.17	0.01	0.0001
Cu	1.58	0.09	0.0012
Fe	86.46	4.95	0.0653
Mg	112.05	6.41	0.0846
Mn	0.46	0.03	0.0003
Ni	0.15	0.01	0.0001
P	934.57	53.47	0.7057
K	42.58	2.44	0.0322
Si	0.82	0.05	0.0006
Na	2.61	0.15	0.0020
Sr	2.69	0.15	0.0020
Zn	4.66	0.27	0.0035
Total	1747.91	100.00	1.30

It should be pointed out that the samples activated by 1 h were selected for the characterization in order to compare the present results mainly against textural results obtained in a previous work related with the synthesis of AC from the Apamate wood [16] as we discuss below.

3.3. Characterization of carbons

3.3.1. FTIR and XPS

FTIR is mainly used as a qualitative technique for the study of the surface chemical functional groups on activated carbon. Since

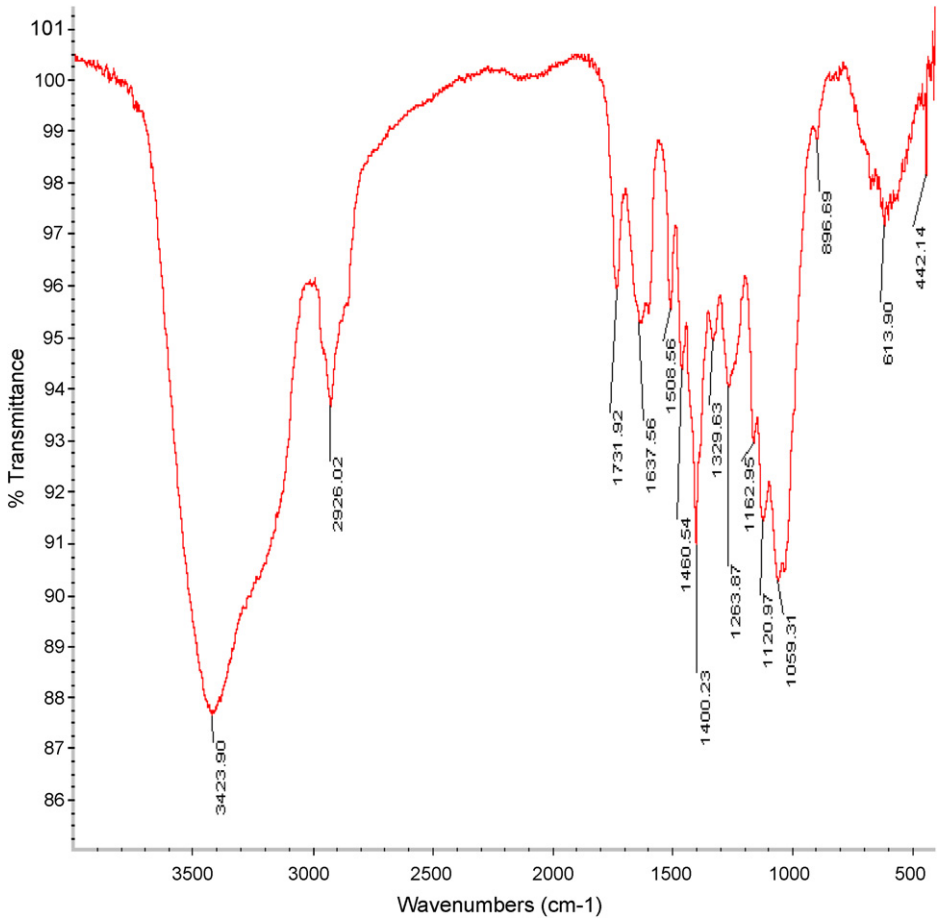

Fig. 3. FTIR spectra of Algarroba wood.

carbon materials are black materials, they absorb almost all of the radiation in the visible spectrum and the peaks obtained in FTIR are commonly a sum of the interactions of different types of groups. However, some interesting features can be obtained from this technique. The FTIR spectra of Algarroba is show in Fig. 3 and in supplementary material the FTIR spectra of some selected carbon materials are included for comparative purposes. A summary of the functional organic groups detected in this wood is compiled in Table 3. A strong absorption peak at about 3424 cm^{-1} and another peak at 1638 cm^{-1} can be assigned to O–H vibrations suggesting the presence of phenol groups. Other important peaks were detected about 2926 cm^{-1}, 1731 cm^{-1} and between 1510 and 1600 cm^{-1} are these peaks are assigned to aliphatic C–H vibrations, carbonyl of lactones, and aromatic rings from lignin, respectively [34,35].

Tables 4 and 5 compile the results of the functional groups detected by FTIR on the surface of carbons prepared under CO_2 and N_2 flows, respectively. Comparison of these tables shows that the predominant groups detected were the carboxylic acids, phenols and ethers groups. Phenol was the main acid surface group detected at low temperatures up to 450 °C under both atmospheres. This result was expected because the main peak detected in the FTIR spectra of the Algarroba wood was phenol group (Fig. 3). It should be remarked that at higher temperatures than 600 °C, carboxylic acids and phenol were not detected indicating a less hydrophilic behavior on the carbon samples in agreement with previous results obtained in the synthesis of other carbon materials [16,36,37].

Fig. 4 shows the XPS spectra in the region O1s of the AC prepared under CO_2 flow at 450 °C (Fig. 4A) and 900 °C (Fig. 4B). Both spectra show clear differences. A summary of the functional groups detected from the XPS analysis in the region O1s for the AC prepared under CO_2 and N_2 flows are presented in Tables 6 and

Table 3
Summary of FTIR results of Algarroba wood.

Functional organic groups	Assignment of absorption bands (cm^{-1})
Carboxylic acid	3200; 1460; 1400; 1117
Lactone	1742; 1158
Phenol	3406; 1400
Ether	1276
Aliphatic groups	2920
Aromatic rings	1629; 892; 774

Table 4
Functional groups detected by FTIR on AC prepared after 1 h reaction under CO_2 flow.

Temperature (°C)	Carboxylic acid	Phenol	Ether
200	√	√	√
250	√	√	√
300	√	√	√
350	×	√	√
450	×	√	√
600	×	×	√
700	×	×	√
800	×	×	√
900	×	×	√

Table 5
Functional groups detected by FTIR on AC prepared after 1 h reaction under N_2 flow.

Temperature (°C)	Carboxylic acid	Phenol	Ethers
200	√	√	√
250	√	√	√
300	√	√	√
350	√	√	√
450	×	√	√
600	×	×	√
700	×	×	√
800	×	×	√
900	×	×	√

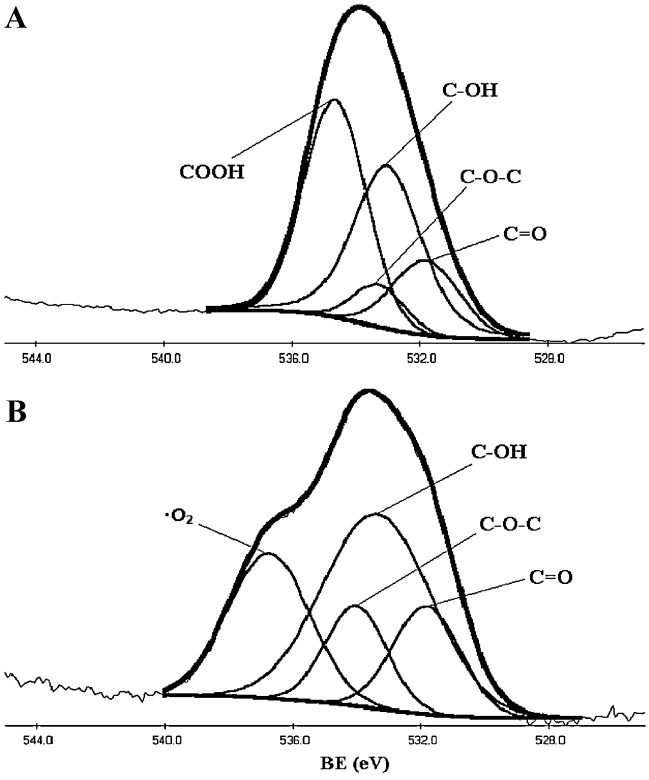

Fig. 4. XPS spectra of 1sO region of some selected carbons activated under CO_2 flow. (A) 450 °C, (B) 700 °C and (C) 900 °C.

7, respectively. For example, AC prepared under CO_2 flow developed carbonyl groups (531.5–532.6 eV) in any of the temperatures while for the case of AC prepared under N_2 flow, the carbonyl was detected at temperatures higher than 700 °C. This result suggests that the CO_2 reacts with the wood even at low temperature to form carbonyl groups on the surface of carbon materials. Phenol and ether groups (533.0–534.1 eV) [36] were also detected in both cases (Tables 6 and 7) in agreement with the FTIR spectra (Tables 4 and 5). The XPS spectrum in Fig. 4A is highly symmetric while the XPS spectrum in Fig. 4B shows a broad shoulder at high binding energy. Fig. 4 also shows the resolved analysis of XPS spectra in the region O1s into four individual peaks. These peaks correspond to the different functional groups detected on the carbon surface. It should be pointed out that at temperatures higher than 600 °C, a broad peak at binding energies between 534.3 and 537.0 eV (Fig. 4B) suggest the presence of chemisorbed water and/or oxygen [38] on carbons. The formation of molecular oxygen radical ($^{\bullet}O_2$) has been proposed by Barr [39]. We also suggest that the peak about 536.7 eV (Fig. 4B) corresponds to this oxygen radical in agreeing with the fact that carbons prepared at high temperatures by physical activation or by pyrolysis commonly are characterized by basic surface pH [16,36,37]. In addition, it is difficult to differentiate between carbons prepared by physical activation or pyrolysed carbons when high temperatures are employed.

XPS spectra in the O1s region (Fig. 4) showed important peaks about 531 eV. Beside the conventional C=O functional group, some authors [37,39] attribute this peak to metal oxides when the chemical composition of the precursor wood is important as in the present case (>1 wt%). It can be suggested that under N_2 flow the particles of metallic oxide need higher temperatures to spread up to the carbon surface in the comparison of CO_2, which can react from temperatures moderated to remove hetero atoms (O and H) of the wood. Finally, it can be seen from Table 8, that the higher the temperature of activation or pyrolysis the more basic is the surface of the carbon. It can be inferred from the pH_{PZC} that surface of carbons evolutes from a soft acid surface to a basic one in agreement with the changes in the oxygenated functional groups detected by FTIR and XPS discussed above. In other words, the higher the temperature of preparation the more hydrophobic behavior of carbons is expected.

3.3.2. SEM

Fig. 5 shows the SEM images of selected AC prepared under CO_2 and N_2 flow. SEM images show some white dots that have been

Table 6
Summary of functional carbon groups detected from XPS analysis in the O1s region for the AC prepared under CO_2 flow by 1 h.

Temperature (°C)	Metallic oxides	Carbonyl	Phenol and ethers	Quimisorbed oxygen or water
350	×	√	√	×
450	×	√	√	×
600	√	√	√	×
700	√	√	√	×
800	√	√	√	√
900	√	√	√	√

Table 7
Summary of oxide carbon groups detected from XPS analysis in the O1s region for the AC prepared under N_2 flow by 1 h.

Temperature (°C)	Metallic oxides	Carbonyl	Phenol and ethers	Quimisorbed oxygen or water
350	×	×	√	×
450	×	×	√	×
600	×	×	√	×
700	×	√	√	×
800	√	√	√	√
900	√	√	√	√

Table 8
BET surface area (S_{BET}) and pH_{PZC} of carbons prepared from Algarroba (Alg) under CO_2 and N_2 flow by 1 h and a comparison against those obtained from Apamate (Apa).

T (°C)	S_{BET} CO_2 (m^2/g)	pH_{PZC} AC_{CO_2}	S_{BET} N_2 (m^2/g)	pH_{PZC} AC_{N_2}
Alg-350	92 ± 1	5.9	34 ± 1	5.8
Alg-450	350 ± 7	6.1	220 ± 6	5.9
Alg-600	870 ± 17	7.0	497 ± 1	6.9
Alg-700	1038 ± 28	7.8	527 ± 2	7.7
Alg-800	1167 ± 31	8.3	549 ± 2	7.8
Alg-900	752 ± 20	8.9	471 ± 12	8.3
Apa-450[a]	352 ± 5	6.3	31 ± 5	6.1
Apa-600[a]	426 ± 13	7.2	360 ± 12	7.1
Apa-700[a]	570 ± 14	8.0	388 ± 13	7.9
Apa-800[a]	770 ± 16	8.5	519 ± 15	8.5
Apa-900[a]	548 ± 21	9.1	590 ± 13	8.9

[a] Results obtained from the Apamate wood at the same experimental conditions [16].

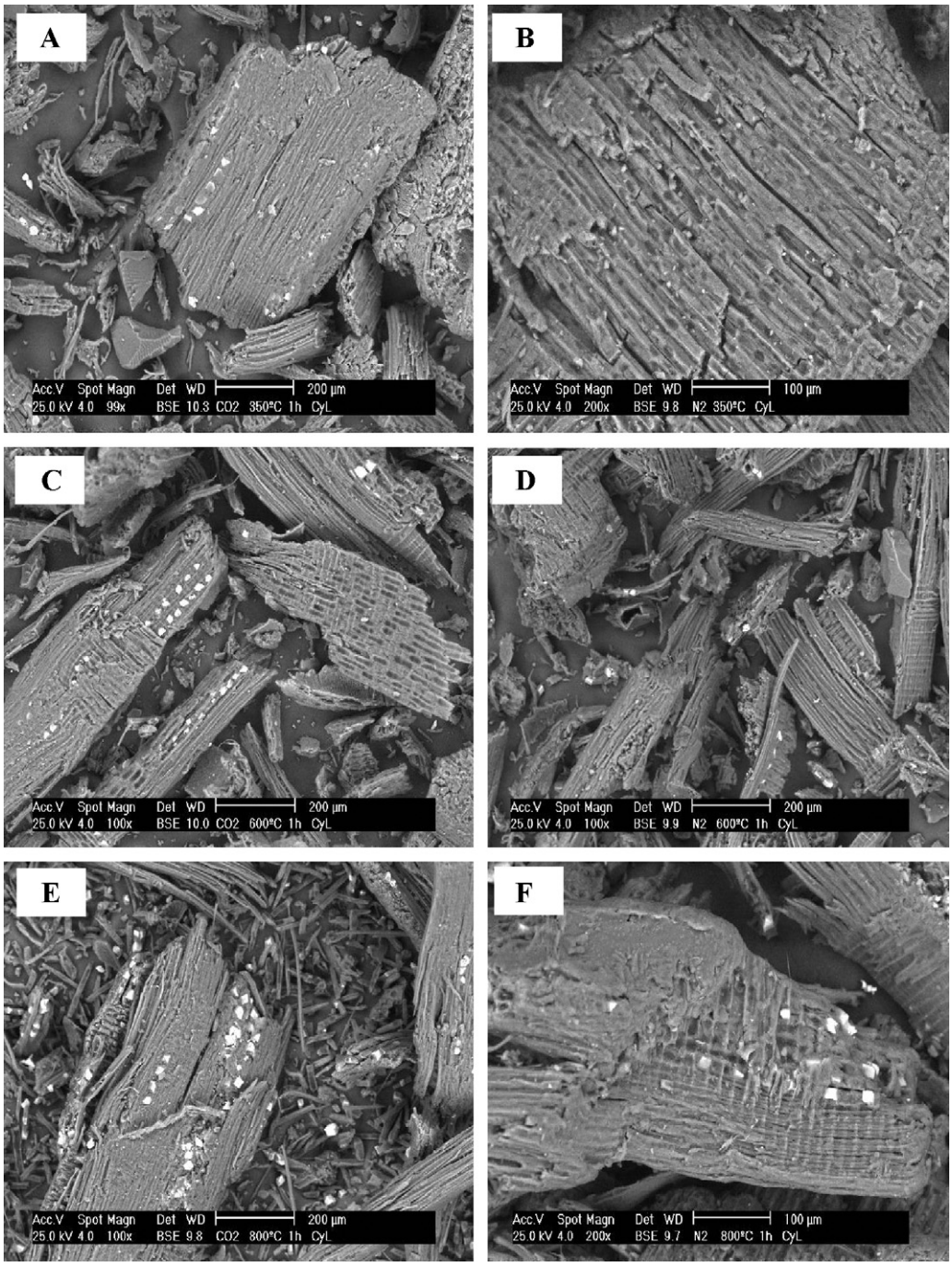

Fig. 5. SEM images of selected activated carbons. (A) CO_2, 350 °C, (B) N_2, 350 °C, (C) CO_2, 600 °C, (D) N_2, 600 °C, (E) CO_2, 800 °C and (F) N_2, 800 °C.

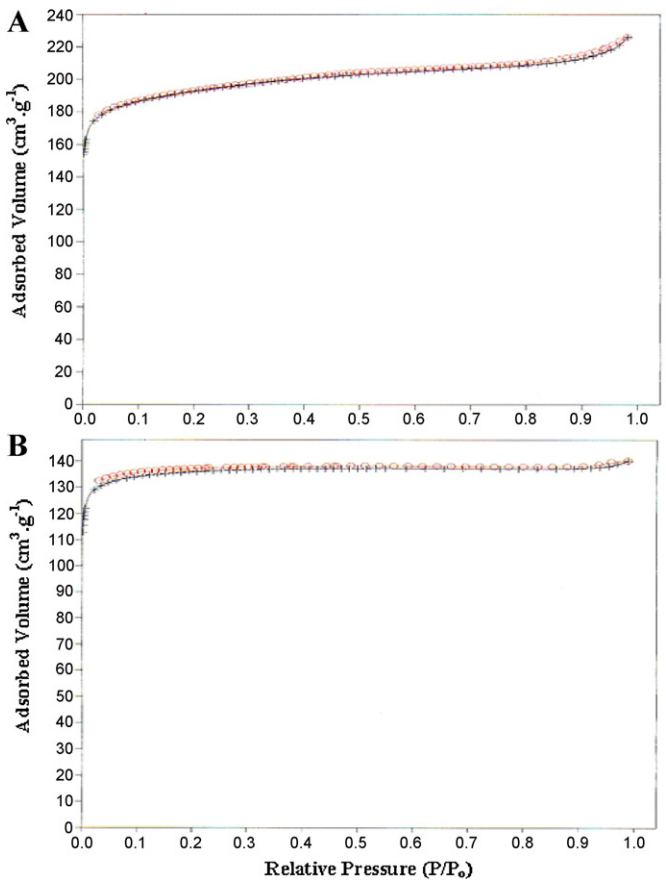

Fig. 6. Adsorption–desorption N_2 isotherm of AC prepared at 800 °C by 1 h. (A) Under CO_2 flow and (B) under N_2 flow.

associated with the inorganic composition of wood. AC particles are in a micrometer scale in agreement with sieving performed. Independently of the gas and activation temperature, AC showed a cellular fibrous morphology. SEM images suggest that the present activated carbons are constituted by an interconnected channel framework in concordance with the fact that the precursor is constituted by a fibrous structure. For example, Fig. 5C indicates that under CO_2 flow, even at moderate temperatures (600 °C), an incipient activation occur in spite of this temperature is lower than that commonly considered as the critical temperature for the spontaneous activation under CO_2 flow (about 690 °C) [29]. Similar tendencies of an interconnected porous system as a function of temperature have been reported for the case of activated fibers obtained from rayon fibers [40] and for activated carbons obtained from almond shells [41].

3.3.3. Texture of AC

For the materials prepared at temperatures higher than 600 °C, the adsorption–desorption N_2 isotherms of carbon prepared under CO_2 and N_2 flow, showed very similar trends characteristic of a micropore framework as suggest Fig. 6 and figures in supplementary material. Fig. 6 shows the analysis for two selected carbons prepared at 800 °C by 1 h under CO_2 and N_2 flow, denoted AC_{CO_2} and AC_{N_2}, respectively. Both isotherms correspond to a type I indicating that the framework is mainly composed by micropores. A summary of BET surface areas (S_{BET}) of AC prepared from Algarroba (hard wood) is compiled in Table 8 and results obtained from Apamate (soft wood) at the same experimental conditions [16] are also shown in Table 8 for comparative purposes. In general, results obtained from Algarroba and Apamate followed very similar trends. As expected, BET surface area of AC prepared under CO_2 flow was higher than under N_2. It must be noted that a maxima in the BET surface area was obtained at 800 °C, both under CO_2 and N_2 flow. This temperature is the same than that we have found before [16] for the preparation of AC from the sawdust of Apamate [16] and for the activation of carbon foams obtained from the controlled pyrolysis of saccharose under CO_2 or N_2 flow [30]. Porosimetry parameters such as micropore area ($\mu pore_{area}$), micropore volume ($\mu pore_{volume}$), total volume or pore (V_{tot}) and pore diameter (W_{pore}) are showed in Tables 9 and 10 for the AC obtained under CO_2 and N_2 flow, respectively. It can be seen that the higher the activation temperature the higher the micropores volume ($\mu pore_{volume}$) and the higher the total volume of pore of AC. For the micropore area ($\mu pore_{area}$), a maximum is reached at 800 °C in agreement with the BET surface area. In most of cases, the microporous area contributes with about 90% of the total surface area. In addition, it can be seen from Tables 9 and 10 that the higher the final temperature of activation the lower the mean width of pore (W_{pore}). For temperatures between 350 and 450 °C macroporous and mesoporous carbons were obtained, respectively; whereas between 600 and 800 °C microporous were obtained. A carefully analysis of mesopore volume compiled in Tables 9 and 10 showed that in spite of the framework of the carbon materials is mainly micropore, the samples prepared by gasification with CO_2 showed higher contribution in the mesopore range than samples prepared under N_2 flow. This was expected because as indicated above, CO_2 reacts effectively with the carbon at temperatures higher than 600 °C. In general, the mean pore diameter decreases monotonically with the increase of the activation or pyrolysis temperature. This could be the consequence of a pseudo-graphitization of the graphene sheets, in spite the present maxima temperature is 900 °C, clearly lower than that require for this phenomena. The mean pore diameter was lower for the AC obtained under N_2 flow than those obtained under CO_2 atmosphere in any of the temperatures studied. For example, at 350 °C, the mean macropore diameter on N_2 flow was about the half than that on CO_2 flow (922 against 1815 Å). This trend is the same for the temperature where mesoporous were obtained (450 °C), and also in the range (600–900 °C) where micropore AC were obtained. It should be pointed out that at 900 °C the lowest mean width of pore of about 6.7 Å (Table 9) and 5.3 Å (Table 10) were obtained under CO_2 and N_2 flows, respectively. These AC can be classify as an ultramicroporous AC which have shown several potential applications such as a double layer capacitor and electrode material [42], as a separation membrane [43], as catalytic support for the hydrogen production from the dry methane reforming [20,21,44,45], and as an efficient adsorbent for the hydrogen uptake and storage [46].

3.4. General discussion

We present here a first part of a major research showing some insights about the design of both textural and functional groups on the surface of AC. It can be summarized that in this work, a hydrophobic and ultramicroporous AC can be prepared by controlling the temperature and atmosphere of the thermal degradation of waste biomass. The potential of these AC, mainly in the industry and in environmental green chemistry applications by cata- and photocatalytic heterogeneous reactions will be presented in the next two works. It should be pointed out that carbon derived materials obtained from sawdust of wood contain lower ash content that those prepared from other lignocellulosic materials such as agroindustrial bio-wastes and clearly much lower than those obtained from petroleum precursors. This is one of the reasons why activated carbon materials prepared from sawdust of wood has been employed successfully in catalytic heterogeneous reactions [1]. For example, Laine et al. [11,12] have showed that pore volume of activated carbon supports play a synergistic role upon

Table 9
Micropore area ($\mu pore_{area}$), micropore volume ($\mu pore_{volume}$), mesopore volume ($mpore_{volume}$), total pore volume (V_{tot}) and mean width of pore (W_{pore}) of AC prepared by activation under CO_2 flow by 1 h.

T (°C)	$\mu pore_{area}$ (m^2/g)[a]	$\mu pore_{volume}$ (cm^3/g)[b]	$mpore_{volume}$ (cm^3/g)[b]	V_{tot} (cm^3/g)[c]	W_{pore} (Å)[c]
350	–[d]	–[d]	–[d]	0.030	1815
450	326.7	0.100	0.007	0.107	54.5
600	624.1	0.241	0.095	0.336	20.6
700	892.0	0.411	0.067	0.478	20.0
800	1003	0.462	0.076	0.538	18.6
900	645.7	0.573	0.094	0.667	6.72

[a] Obtained by HJ method.
[b] Obtained by HJ method.
[c] Obtained by HK method.
[d] Not estimated.

the activity and selectivity of NiMo catalysts the in thiophene hydrodesulphurization. Also, our group has showed that pore size distribution clearly influence the catalytic activity of Ni and NiMo catalysts in the ethylene hydrogenation [9] and the kinetics of coke deposition [10]. Also, our group have showed in different works about synthesis of activated carbons by physical activation or by pyrolysis [16], and by chemical activation [17] that the pore size distribution and surface area of activated carbons remarkably affects the photoactivity of TiO_2 in the photocatalytic detoxification of 4-chlorophenol. In addition, we have showed that textural properties of activated carbon clearly influence the selectivity of main intermediate products detected during the aromatic molecules as phenol and 2,4-dichlorophenoxiacetic acid [13,14] and more recently on 4-chlorophenol [47,48] and 2-propanol [49] photooxidations. In this sense, Fig. 7 shows the influence of the two carbons prepared at 800 °C by 1 h upon the phenol adsorption and on the photo efficiency of TiO_2 in the phenol photo detoxification under UV-irradiation. It can be seen from Fig. 7 that any of two TiO_2–AC binary materials adsorbed higher phenol (after 15 min adsorption in the dark). This enhancement in phenol molecules around photoactive TiO_2 enhances the photo efficiency of the semiconductor as can also be seen in Fig. 7. This enhances has been attributed to the presence of a common contact interface between TiO_2 and AC that make possible a continuous transfer of the species from the AC to the TiO_2 surface [49]. Our present enforces are aimed to prepare hierarchically macro–meso–micro porous carbon materials to study the influence of pore size distribution on the selectivity of NiMo catalysts in hydrocracking reactions and to verify the presence of confinement effects on the selectivity of hydrocracking consequence of specific pore size an pore volume of the support such as in the case of zeolites [50,51]. We do believe that the present results regarding the pyrolysis of sawdust of a hard wood as Algarroba consists of essentially 3 different zones is a very important finding and deserve to be studied carefully. A better explanation for the present results where the reaction rates rather decreased with the increasing temperature from 350 to 600 °C could be due to the

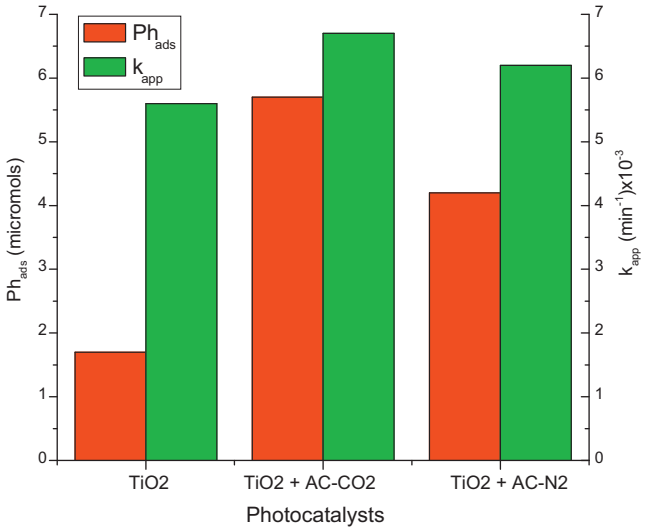

Fig. 7. Summary of kinetic results of phenol adsorption in the dark (Ph_{ads}) and first-order apparent rate-constants (k_{app}) of phenol photodegradation under UV-irradiation.

presence of different chemical structures of the starting materials at zero holding time after heating up to the set temperatures (i.e., 350, 400 and 600 °C). Therefore, the estimation of kinetic parameters from data of modulated thermogravimetric analysis is required to better understand the correlation of the influence of each pyrolysis zone on the pore size distribution and pore volume of carbon materials. In addition, the influence of ashes of lignocellulosic carbon precursors and the influence of additives (chemical activators) that can play the role of catalysts to improve the textural properties are necessary to clarify the significance of the present results. In this way, our groups have already reported preliminary studies regarding the influence of the pyrolysis atmosphere [52] and the effect of

Table 10
Micropore area ($\mu pore_{area}$), micropore volume ($\mu pore_{volume}$), mesopore volume ($mpore_{volume}$), total pore volume (V_{tot}) and mean width of pore (W_{pore}) of AC prepared by activation under N_2 flow by 1 h.

T (°C)	$\mu pore_{area}$ (m^2/g)[a]	$\mu pore_{volume}$ (cm^3/g)[b]	$mpore_{volume}$ (cm^3/g)[b]	V_{tot} (cm^3/g)[c]	W_{pore} (Å)[c]
350	–[d]	–[d]	–[d]	0.016	922
450	201.7	0.101	0.010	0.111	43.3
600	449.1	0.172	0.018	0.190	16.3
700	494.0	0.188	0.013	0.201	15.8
800	515.4	0.195	0.013	0.208	15.8
900	454.8	0.223	0.008	0.231	5.33

[a] Obtained by HJ method.
[b] Obtained by HJ method.
[c] Obtained by HK method.
[d] Not estimated.

chemical additives [53] on the topological organization of carbon materials obtained from the controlled pyrolysis of saccharose.

4. Conclusions

AC was prepared from the sawdust of wood by physical activation and pyrolysis under CO_2 and N_2 flow, respectively. Maxima BET surface area was obtained at 800 °C, both under CO_2 and N_2 atmospheres to then decrease at higher temperatures of activation. IR and XPS suggest that the higher the activation temperature the more basic is the functional groups on surface of carbons. Porosimetry showed that the higher the activation temperature the higher the micropores volume and the higher the micropore surface of AC. The higher the activation temperature the lower the pore diameter obtaining an ultramicroporous activated carbon at 900 °C. It can be concluded that mean pore width and functionalization on the surface of AC can be easily controlled and this feature permits to think in waste biomass as a potential source for the synthesis of carbon materials with different and potential modern applications.

Acknowledgement

J. Matos thanks to the Ministry of Science and Technology for financial support.

Appendix A. Supplementary data

Supplementary data associated with this article can be found, in the online version, at doi:10.1016/j.jhazmat.2011.09.046.

References

[1] F. Rodríguez-Reinoso, M. Molina-Sabio, Activated carbons from lignocellulosic materials by chemical and/or physical activation: an overview, Carbon 30 (1992) 1111–1118.
[2] K. Gergova, S. Eser, Effects of activation method on the pore structure of activated carbons from apricot stones, Carbon 34 (1996) 879–888.
[3] F. Rodríguez-Reinoso, The role of carbon materials in heterogeneous catalysis, Carbon 36 (1998) 159–175.
[4] M. Jagtoyen, F.F. Derbyshire, Activated carbons from yellow poplar and white oak by H_3PO_4 activation, Carbon 36 (1998) 1085–1097.
[5] N. Kannan, G. Rengasamy, Comparison of cadmium ion adsorption on various carbons, Fresenius Environ. Bull. 11 (2002) 160–164.
[6] N. Tancredi, N. Medero, F. Möller, J. Piriz, C. Plada, T. Cordero, Phenol adsorption onto powdered and granular activated carbon, prepared from Eucalyptus wood, J. Colloid Interface Sci. 279 (2004) 357–363.
[7] N. Kannan, G. Rengasamy, Comparison of cadmium ion adsorption on various activated carbons, Water Air Soil Pollut. 163 (2005) 185–201.
[8] T. Tay, S. Ucar, S. Karagöz, Preparation and characterization of activated carbon from waste biomass, J. Hazard. Mater. 165 (2009) 481–485.
[9] J. Matos, J. Laine, J.L. Brito, Activated carbon supported Ni–Mo: effects of pretreatments and composition on catalyst reducibility and on ethylene conversion, Appl. Catal. A: Gen. 152 (1997) 27–42.
[10] J. Matos, J. Laine, Ethylene conversion on activated carbon supported NiMo catalysts: effect of the support, Appl. Catal. A: Gen. 241 (2003) 25–38.
[11] J. Laine, F. Severino, M. Labady, J. Gallardo, The synergistic participation of the support in sulfided Ni–Mo/C hydrodesulfurization catalysts, J. Catal. 138 (1992) 145–149.
[12] J. Laine, F. Severino, M. Labady, Optimum Ni composition in sulfided Ni–Mo hydrodesulfurization catalysts: effect of the support, J. Catal. 147 (1994) 355–357.
[13] J. Matos, J. Laine, J.-M. Herrmann, Synergy effect in the photocatalytic degradation of phenol on a suspended mixture of titania and activated carbon, Appl. Catal. B: Environ. 18 (1998) 281–291.
[14] J. Matos, J. Laine, J.-M. Herrmann, Effect of the type of activated carbons on the photocatalytic degradation of aqueous organic pollutants by UV-irradiated titania, J. Catal. 200 (2001) 10–20.
[15] J. Matos, J. Laine, J.-M. Herrmann, D. Uzcategui, J.L. Brito, Influence of activated carbon upon titania on aqueous photocatalytic consecutive runs of phenol photomineralization, Appl. Catal. B: Environ. 70 (2007) 461–469.
[16] T. Cordero, C. Duchamp, J.-M. Chovelon, C. Ferronato, J. Matos, Surface nanoaggregation and photocatalytic activity of TiO_2 on H-type activated carbons, Appl. Catal. B: Environ. 73 (2007) 227–235.
[17] T. Cordero, C. Duchamp, J.-M. Chovelon, C. Ferronato, J. Matos, Influence of L-type activated carbons on photocatalytic activity of TiO_2 in 4-chlorophenol photodegradation, J. Photochem. Photobiol. A: Chem. 191 (2007) 122–131.
[18] A. Dufour, A. Celzard, V. Fierro, E. Martin, F. Broust, A. Zoulalian, Catalytic decomposition of methane over a wood char concurrently activated by a pyrolysis gas, Appl. Catal. A: Gen. 346 (2008) 164–173.
[19] A. Dufour, A. Celzard, B. Ouartassi, F. Broust, V. Fierro, A. Zoulalian, Effect of the micropores diffusion on kinetics of CH_4 decomposition over a wood-derived carbon catalyst, Appl. Catal. A: Gen. 360 (2009) 120–125.
[20] J. Matos, K. Díaz, V. García, T. Cordero, J.L. Brito, Methane transformation in presence of carbon dioxide on activated carbon supported nickel–calcium catalysts, Catal. Lett. 109 (2006) 163–169.
[21] K. Díaz, V. García, J. Matos, Activated carbon supported Ni–Ca: influence of reaction parameters on activity and stability of catalyst on methane reformation, Fuel 86 (2007) 1337–1344.
[22] D. Mohan, C.U. Pittman, P.H. Steele, Pyrolysis of wood/biomass for bio-oil: a critical review, Energy Fuels 20 (2006) 848–889.
[23] C. Di Blasi, C. Branca, Kinetics of primary product formation from wood pyrolysis, Ind. Eng. Chem. Res. 40 (2001) 5547–5556.
[24] C. Branca, C. Di Blasi, Kinetics of the isothermal degradation of wood in the temperature range 528–708K, J. Anal. Appl. Pyrolysis 67 (2003) 207–219.
[25] E. Schröder, K. Thomauske, C. Weber, A. Hornung, V. Tumiatti, Experiments on the generation of activated carbon from biomass, J. Anal. Appl. Pyrolysis 79 (2007) 106–111.
[26] J. Matos, C. Nahas, L. Rojas, M. Rosales, Open Environ. Eng. J. 4 (2011) 1–10.
[27] J. Laine, A. Calafat, LabadyF M., Preparation and characterization of activated carbons from coconut shell impregnated with phosphoric acid, Carbon 27 (1989) 191–195.
[28] M. Sefain, S. El-Kalyoubi, N. Shukry, Thermal behavior of holo- and hemicellulose obtained from rice straw and bagasse, J. Polym. Sci.: Polym. Chem. 23 (1985) 1569–1577.
[29] T. Wigmans, Industrial aspects of production and use of activated carbons, Carbon 27 (1989) 13–22.
[30] J. Matos, M. Labady, A. Albornoz, J. Laine, J.L. Brito, Topological organization and textural changes of carbon macro-networks submitted to activation with N_2 and CO_2, J. Mater. Sci. 39 (2004) 3705–3716.
[31] F.E. Huggins, G.P. Huffman, N. Shah, F.W. Lytle, R.B. Greegor, R.G. Jenkins, In Situ XAFS studies of catalyzed pyrolysis and gasification reactions of lignite, Phys. B: Condens. Matter 158 (1989) 178–179.
[32] S.G. Chen, R.T. Yang, Unified mechanism of alkali and alkaline earth catalyzed gasification reactions of carbon by CO_2 and H_2O, Energy Fuels 11 (1997) 421–427.
[33] J. Rodriguez, F. Ruette, J. Laine, Molecular modeling of micropores in activated carbon, Carbon 32 (1994) 1536–1537.
[34] N.L. Owen, D.W. Thomas, Infrared studies of hard and soft woods, Appl. Spectrosc. 43 (1989) 451–455.
[35] E. Fuente, J.A. Menéndez, M.A. Diez, D. Suárez, M.A. Montes-Morán, Infrared spectroscopy of carbon materials: a quantum chemical study of model compounds, J. Phys. Chem. B 107 (2003) 6350–6359.
[36] A. Swiatkowski, H. Grajek, M. Pakula, S. Biniak, Z. Witkiewicz, Voltammetric studies of the gradual thermal decomposition of activated carbon surface oxygen complexes, Colloids Surf. A: Phys. Eng. Aspects 208 (2002) 313–320.
[37] A. Terzyk, The influence of activated carbon surface chemical composition on the adsorption of acetaminophen (paracetamol) in vitro. Part II. TG. FTIR, and XPS analysis of carbons and the temperature dependence of adsorption kinetics at the neutral Ph, Colloids Surf. A: Phys. Eng. Aspects 177 (2001) 23–45.
[38] H. Valdés, M. Sánchez-Polo, J. Rivera-Utrilla, C.S. Zaror, Effect of ozone treatment on surface properties of activated carbon, Langmuir 18 (2002) 2111–2116.
[39] T.L. Barr, Recent advances in X-ray photoelectron spectroscopy studies of oxides, J. Vac. Sci. Technol. A 9 (1991) 1793–1805.
[40] C. Basquet, B. Rousseau, H. Estrade-Szwarckopt, P. Le Cloirec, Observation of activated carbon fibres with SEM and AFM correlation with adsorption data in aqueous solution, Carbon 38 (2000) 407–422.
[41] A. Marcilla, S. García-García, M. Asensio, J.A. Conesa, Influence of thermal treatment regime on the density and reactivity of activated carbons from almond shells, Carbon 38 (2000) 429–440.
[42] J. Koresh, A. Soffer, Double layer capacitance and charging rate of ultramicroporous carbon electrodes, J. Electrochem. Soc. 124 (1977) 1379–1385.
[43] C.W. Jones, W.J. Koros, Characterization of ultramicroporous carbon membranes with humidified feed, Ind. Eng. Chem. Res. 34 (1995) 158–163.
[44] J. Matos, M. Rosales, C. Urbina de Navarro, G. González, Medusa-like carbon nanotubes formed during dry methane reforming on activated carbon-supported Ni–Ca catalyst, Acta Microsc. 18 (2009) 322–332.
[45] J. Matos, M. Rosales, G. González, C. Urbina de Navarro, Changes on texture and crystalline phase of activated carbon-supported Ni–Ca catalyst during dry methane reforming, Open Mater. Sci. J. 4 (2010) 125–132.
[46] V.V. Bhata, C.I. Contescu, N.C. Gallego, F.S. Baker, A typical hydrogen uptake on chemically-activated, ultramicroporous carbon, Carbon 48 (2010) 1331–1340.
[47] J. Matos, A. García, T. Cordero, J.-M. Chovelon, C. Ferronato, Eco-friendly TiO_2–AC photocatalyst for the selective photooxidation of 4-chlorophenol, Catal. Lett. 130 (2009) 568–574.
[48] J. Matos, A. García, P.S. Poon, Environmental green chemistry applications of nanoporous carbons, J. Mater. Sci. 45 (2010) 4934–4944.

[49] J. Matos, E. García-López, L. Palmisano, A. García, G. Marci, Influence of activated carbon in TiO_2 and ZnO mediated photo-assisted degradation of 2-propanol in gas–solid regime, Appl. Catal. B: Environ. 99 (2010) 170–180.
[50] E. Benazzi, L. Leite, N. Marchal-George, H. Toulhoat, P. Raybaud, New insights into parameters controlling the selectivity in hydrocracking reactions, J. Catal. 217 (2003) 376–387.
[51] H. Toulhoat, P. Raybaud, E. Benazzi, Effect of confinement on the selectivity of hydrocracking, J. Catal. 221 (2004) 500–509.
[52] J. Matos, J. Laine, A carbon macro-network from the controlled pyrolysis of saccharose, J. Mater. Sci. Lett. 17 (1998) 649–651.
[53] J. Matos, M. Labady, A. Albornoz, J. Laine, J.L. Brito, Catalytic effect of KOH on textural changes of carbon macronetworks by physical activation, J. Mol. Catal. A: Chem. 228 (2005) 189–194.